Measurements of Velocity and Vorticity Fields Around a Pitching Swept Wing

P. B. Rymarz*
ESCO Corporation, Portland, Oregon 97210
and
B. R. Ramaprian†
Washington State University, Pullman, Washington 99164-2920

Introduction

MOST studies reported on dynamic stall in three-dimensional flows pertain to swept and unswept wings of finite aspect ratio, wing–body junctions, and delta wings. All these flows can be classified as strongly three-dimensional. The configuration studied in the present case approximates to an infinite wing of small sweep pitched about an axis perpendicular to the freestream. The flow in this case is quasi-two-dimensional when the wing is stationary, but it becomes three-dimensional when the wing is pitched. The three-dimensionality of the unsteady flow is a consequence of the selected pitch axis geometry that results in a spanwise variation of the location of the pitch axis.

The experiments were conducted in an open-surface water channel, described by Conger and Ramaprian.[1] The wing model is of NACA 0015 profile and has a 30-cm (1-ft) chord (c), a 61-cm (2-ft) span, and a back-sweep angle of 15 deg. The wing with its transparent end plates is suspended vertically in the water channel and is rotated about a vertical axis (the pitching axis) by a computer-controlled stepper motor. Figure 1a shows a schematic of the experimental setup. The wing mounting is such that the pitching axis passes through the $c/4$ (quarter chord) point at the midspan plane. This midplane is arbitrarily designated as the $z = 0$ plane, even though under infinite wing approximation there is no preferred origin for the z axis. Results obtained in this plane are compared with data obtained in earlier experiments in the same facility on an unswept, but otherwise identical, wing pitched about its quarter-chord axis at the same Reynolds number and pitch rate.[2]

Measurements of the instantaneous velocity components V_x and V_y in the streamwise (x) and normal (y) directions, around the suction side of the wing in three different horizontal spanwise planes [midplane and ±5 cm (±2 in.) from midplane], were made by using two-dimensional particle image velocimetry (PIV). The experiments were performed at a freestream velocity (U_∞) of about 32 cm/s (1.07 ft/s) (corresponding to $Re \approx 13.5 \times 10^4$) and a nondimensional pitch rate $\alpha^+ (= \dot{\alpha} c / U_\infty) = 0.075$, where $\dot{\alpha}$ is the constant angular velocity of pitching. Surface pressure data for this wing model and for the same experimental conditions are available from Patterson et al.[3]

To achieve a high spatial resolution of the velocity field, only one-third of the chord (forward, middle, or aft) was photographed during a pitching realization. Each realization consisted of a pitching maneuver from 0 to 33 deg, with photographs taken in 1-deg increments. The results obtained for the three wing regions from three separate pitching realizations were then combined to obtain 4800 vectors to describe the composite flowfield over the entire wing. This procedure resulted in a spatial resolution of about $0.008c$. There was some mismatch between the three realizations in some cases, but these generally did not present any serious difficulties in developing the composite picture. More details of the measurements are given by Rymarz.[4] The velocity data are estimated to have an uncertainty of 4% in all of the regions of the flow except in the immediate vicinity of the wall, where the uncertainty is about 8%, and the vorticity values estimated from the velocity data have an uncertainty of 8% (16% immediately next to the wall).

Results for the Midplane

Figure 1b taken from Ref. 3 shows the lift results for the swept and unswept wings at the same nondimensional pitch rate of 0.075. It also shows lift results for the stationary swept wing. The stationary swept wing of this geometry stalls at 17–18 deg. For the pitching swept wing, the maximum lift is slightly larger and the lift drop-off after dynamic stall is more gradual compared to the unswept wing.

Figure 2 shows a comparison of the contours of spanwise vorticity in the midplane of the swept wing, with the data from corresponding unswept wing experiments from Ref. 2. Because the pitch-axis location is the same in both cases, any differences observed in the flow structure between the swept wing and the unswept wing at this plane are interpreted as due to the three-dimensionality of the unsteady flow over the swept wing.

The flowfields for the two wings were found to be similar at early angles of incidence. At an incidence of 20 deg, both flows were found to exhibit the presence of strong, clockwise (negative), leading-edge vorticity. The vorticity contours were nearly parallel and concentrated next to the wing surface. Figure 2 shows that, as the angle of incidence increases to 22 deg, the swept wing continues to exhibit nearly the same vorticity structure. In the case of the unswept wing, however, a well-defined vortex has formed and the shear layer of negative vorticity has started to move up. The contrast between the two wings becomes stronger as the incidence increases to approximately 24 deg. The shear layer over the unswept wing has definitely moved out and is about to leave the surface, whereas no major separation of the shear layer has occurred over the unswept wing. Finally, at the incidence of 26 deg, the dynamic stall vortex (DSV) has detached from the surface of the unswept wing and has, in fact, partially left the field of view. Figure 1b shows that the lift has reached a maximum at this incidence for the unswept wing. In comparison, the DSV structure of the swept wing (essentially a rolled-up shear layer with a large number of distributed vortices) is still contained and remains near the wall. The lift continues to increase beyond 26 deg (as shown in Fig. 1b). In fact, the interesting features of the flowfield over the swept wing were found still to be completely within the field of view even at 28 deg, when dynamic stall eventually occurred over this wing. The DSV on the unswept wing was found to be completely washed away at this incidence. A careful study of Fig. 2 shows that, although events near the leading edge such as the onset of the leading-edge vortex, shear layer detachment, and growth and liftoff of the DSV structure occur in both cases, all these events occur later over the swept wing.

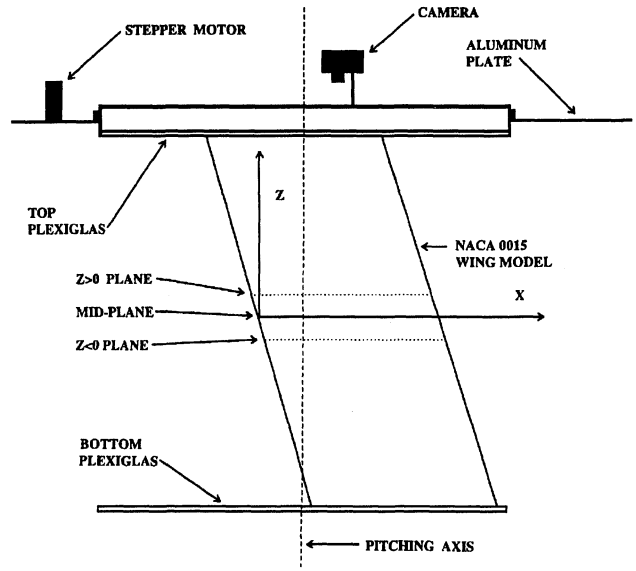

Fig. 1a Schematic of wing model and mounting arrangement.

Received Jan. 18, 1996; presented as Paper 95-2161 at the AIAA 26th Fluid Dynamics Conference, San Diego, CA, June 19–22, 1996; revision received Sept. 12, 1996; accepted for publication Sept. 29, 1996; also published in *AIAA Journal on Disc*, Volume 2, Number 2.

*Design Engineer, 2141 NW 25th Avenue, P.O. Box 10123.
†Professor, School of Mechanical and Materials Engineering, P.O. Box 642920. Member AIAA.

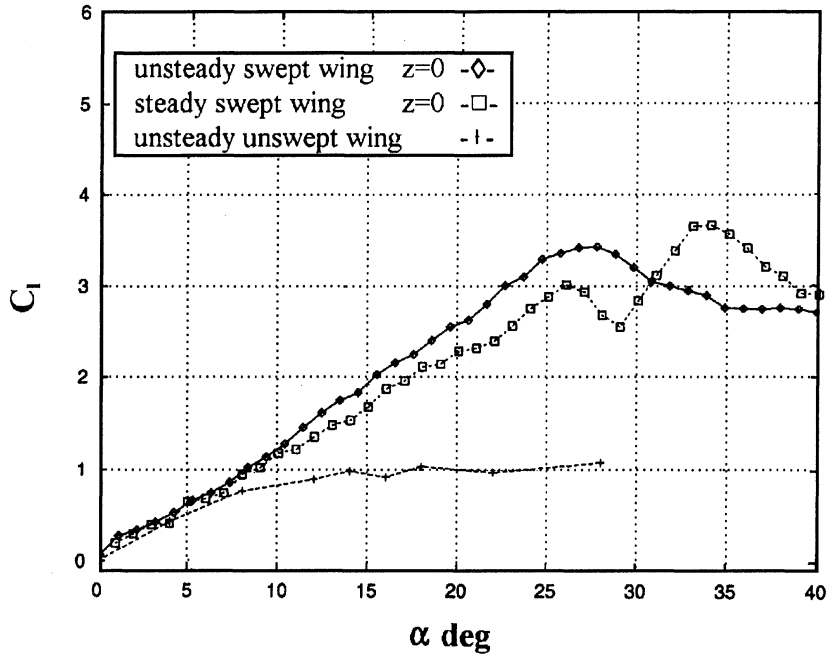

Fig. 1b Lift coefficient vs angle of incidence for swept and unswept wings (from Ref. 3). Reynolds number and pitch rate are the same as in the present experiment.

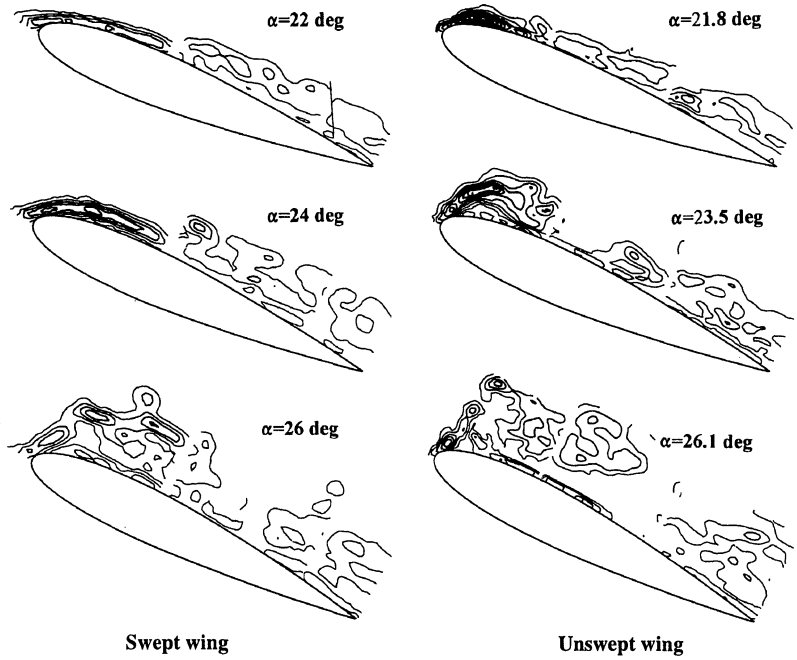

Fig. 2 Contours of instantaneous spanwise vorticity on the suction side of the swept and unswept wings for typical angles of incidence. Results for the swept wing are for the midplane (z = 0). Pitch axis location in both cases, 0.250c.

The second major difference between the swept and unswept wings is the severity with which they seem to stall. In the case of the unswept wing, when dynamic stall occurs at 26 deg, the DSV is abruptly ejected in a direction nearly perpendicular to the chord, resulting in a drastic loss of lift after stall, as shown in Fig. 1b. On the other hand, the loss of vorticity associated with the DSV and, hence, the loss of lift after dynamic stall is gradual in the case of the swept wing. This gradual loss is due both to the distributed nature of vorticity within the DSV and the nearly parallel direction in which it is convected away from the wing.

Comparison Between Different Spanwise Planes

The PIV results indicated similar sequential evolution of the flowfield at different spanwise planes. However, the leading-edge vortex formation, the subsequent evolution of the flow, and the eventual dynamic stall all were found to occur at progressively later incidences as z varied from −5 cm (−2 in.) to +5 cm (+2 in.). Consequently, at an incidence of 26 deg, the main vortex structure at z = +5 cm (+2 in.) was found to be completely contained within the leading-edge region of the flow, whereas in the midplane (z = 0) the vortex structure protruded into the midchord region. The vortex structure at z = −5 cm (−2 in.) showed an even larger growth and spread. The contrast in stall development was found to be even stronger at 28-deg incidence, as shown in Fig. 3. In the uppermost plane [z = +5 cm (+2 in.)], the DSV has formed but vorticity is still largely contained near the surface of the wing and dynamic stall has not yet occurred. In the midplane, the DSV has evolved significantly more. In fact, dynamic stall has just occurred in this plane and lift has reached a maximum as shown in Fig. 1b. In the lowest plane [z = −5 cm (−2 in.)], the DSV has grown very large and has moved farther downstream compared to the midplane. It is therefore clear that the dynamic stall progresses gradually from the bottom toward

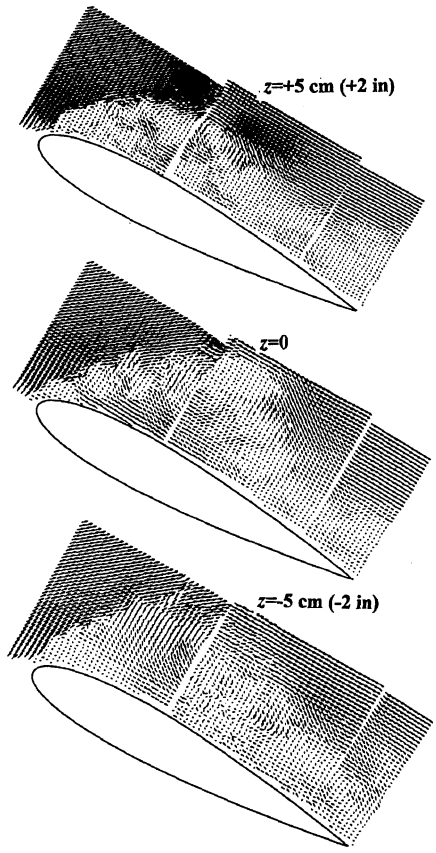

Fig. 3 Comparison of instantaneous velocity vectors in different spanwise planes of the swept wing at an incidence of 28 deg.

the top of the wing. Because the flow stays attached longer as z increases from -5 to $+5$ cm (-2 to $+2$ in.), the vorticity associated with the leading-edge shear layer continues to increase for a longer period of time at higher values of z. Therefore, one can expect the maximum lift to be higher and occur later as z increases. Indeed, the sectional lift data obtained in different spanwise planes in Ref. 3 indicated this behavior.

In the present setup, the distance of the pitch axis from the leading edge varies from $0.208c$ at $z = -5$ cm (-2 in.) to $0.25c$ at $z = 0$ to $0.292c$ at $z = +5$ cm ($+2$ in.). The progressive delay in stall and increase in maximum lift with increasing value of z are somewhat similar to those produced by a similar aftward shift in pitch-axis location in two-dimensional flows. However, the effects observed in the present studies are not merely quasi-two-dimensional. The progressive time delay of events across the wing span effectively causes the DSV front to propagate obliquely (from bottom left toward top right in the present case) over the wing surface as the angle of incidence increases. This explains the gradual washing away of the vorticity (as opposed to its rapid ejection from the surface), thereby preventing a catastrophic loss of overall lift. Flow visualization studies also confirmed the spreading of the stall over the wing surface in this manner.

Although the exact direction of spreading of the DSV and quantitative details associated with it depend on the pitch-axis geometry, the qualitative features of the DSV kinematics such as oblique spreading over the wing surface and gradual washing away of vorticity (leading to a gradual dynamic stall process) resemble the process of open-type separation often observed in steady three-dimensional flows.[5] Hence, the qualitative features of dynamic stall observed in the present studies are probably generic to three-dimensional unsteady flows over all pitching wings.

Acknowledgment

The authors gratefully acknowledge support of this work by the U.S. Air Force Office of Scientific Research through Grant F49620-92-J-0146.

References

[1]Conger, R. N., and Ramaprian, B. R., "Pressure Measurements on a Pitching Airfoil in a Water Channel," *AIAA Journal*, Vol. 32, No. 1, 1994, pp. 108–115.

[2]Oshima, H., and Ramaprian, B. R., "Velocity Measurements over a Pitching Airfoil," *AIAA Journal*, Vol. 35, No. 1, 1997, pp. 119–126.

[3]Patterson, A. K., Rymarz, P. B., and Ramaprian, B. R., "Surface Pressure Measurements on a Pitching Swept Wing in a Water Channel," *AIAA Journal*, Vol. 33, No. 10, 1995, pp. 1871–1879.

[4]Rymarz, P. B., "Measurements of Velocity and Vorticity Fields Around a Pitching Swept Wing," M.S. Thesis, Mechanical and Materials Engineering Dept., Washington State Univ., Pullman, WA, May 1995.

[5]Wang, K. C., "Separation Patterns of Boundary Layer over an Inclined Body of Revolution," *AIAA Journal*, Vol. 10, No. 8, 1972, pp. 1044–1050.

Boundary-Layer Characterization on Moving Walls by an Embedded Laser Velocimetry Technique

M. Pascazio,* J. M. Autric,* D. Favier,† and C. Maresca†
Universités d'Aix-Marseille 1 et 2, 13288 Marseille Cedex 09, France

Nomenclature

c	= chord of the model, m
f	= frequency of oscillation, Hz
H	= integral shape factor, $H = \delta_1/\delta_2$
k	= reduced frequency of oscillation, $c\omega/2U_\infty$
Re	= Reynolds number, $U_\infty c/\nu$
Re_s	= local Reynolds number, $U_e(s, t)s/\nu$
s	= curvilinear distance along the wall from the leading edge, m
t	= time, s
U	= mean velocity tangent to the wall, ms^{-1}
U_e	= mean local external velocity, ms^{-1}
U_∞	= freestream velocity, ms^{-1}
u	= instantaneous tangent velocity (parallel to the wall), ms^{-1}
u'	= fluctuating tangent velocity, ms^{-1}
V	= mean velocity normal to the wall, ms^{-1}
v	= instantaneous velocity normal to the wall, ms^{-1}
y	= distance normal to the model wall, m
α	= instantaneous incidence of the model, deg
α_0	= mean incidence of the model, deg
δ	= boundary-layer thickness, m
δ_1	= integral displacement thickness, m
δ_2	= integral momentum thickness, m
δ_3	= first integral energy thickness, m
δ_3'	= second integral energy thickness, m
ν	= kinematic viscosity, m^2s^{-1}
σ_u	= tangential turbulence intensity, $\sigma_u = \sqrt{\langle u'^2\rangle}/U_e$
ω	= angular frequency, $2\pi f$, $rads^{-1}$
ωt	= phase of the period, deg

Presented as Paper 96-0035 at the AIAA 34th Aerospace Sciences Meeting, Reno, NV, Jan. 15–18, 1996; received Feb. 5, 1996; revision received Sept. 18, 1996; accepted for publication Sept. 29, 1996; also published in *AIAA Journal on Disc*, Volume 2, Number 2.

*Graduate Student, Institut de Recherche sur les Phénomènes hors Équilibre/Laboratoire Aerodynamique Subsonique Instationnaire, Unité Mixte de Recherche 138, Centre National de la Recherche Scientifique, 163, Avenue de Luminy, Case 918.

†Senior Research Scientist, Institut de Recherche sur les Phénomènes hors Équilibre/Laboratoire Aerodynamique Subsonique Instationnaire, Unité Mixte de Recherche 138, Centre National de la Recherche Scientifique, 163, Avenue de Luminy, Case 918. Member AIAA.